Analysis of Reflectometry and Ellipsometry Data from Patterned Structures

M.E. Lee, C. Galarza, W. Kong, W. Sun and F. L. Terry, Jr.
Department of Electrical Engineering and Computer Science, University of Michigan, Ann Arbor, MI. 48109-2122

Specular reflected light techniques, including both single wavelength and spectroscopic versions of ellipsometry and reflectometry, have been used for both etch and growth rate control. However, use of these techniques for process control on products has been limited due to the problems inherent in the analysis of reflected light from patterned structures. In this paper, we examine techniques for the quantitative analysis of data from both highly regular grating structures and from patterns with low local order. We find good quantitative agreement of vector diffraction theory to specular reflection data. We conclude that there is significant promise for the use of specular techniques for in situ monitoring of topography provided that computational speed issues can be improved.

Introduction

High accuracy, high speed, non-invasive wafer state monitors are important for advanced semiconductor process development and control. Reflected light measurements have proven to be very successful for *in situ* monitoring, endpoint detection, and feedback control of vacuum processes on unpatterned substrates. Single wavelength and spectroscopic ellipsometry (1), laser and spectral reflectometry (2,3), and related methods have all been used to demonstrate monitoring accuracies in the ~1nm or better range. However, applications of these methods in actual production have been very limited due to the problems inherent in monitoring patterned structures. Laser reflectometry (4) and laser ellipsometry (5) have been used in some patterned structure monitoring and endpoint detection applications. Recent success in the use of multi-wavelength ellipsometry to monitor and control high density reactive ion etching of digital circuit structures with long pattern repeat distances has been achieved using a scalar theory for modeling the polarization dependent reflection problem (6). However, as expected, these scalar methods are inaccurate on periodic patterns due to strong diffraction effects. Some initial efforts have been made to experimentally and theoretically examine ellipsometry data from gratings (7,8,9). However, quantitative analyses have been limited.

Ex situ applications of diffraction-based measurements (scatterometry) have shown that accurate critical dimensions, thickness, and sidewall shapes can be obtained by analyzing the specular and higher order diffraction intensities vs. angle of incidence (10) or by analyzing the relative intensity of several diffracted orders at a single angle of incidence (11). However, for *in situ* applications, it is often only possible to obtain specular reflection information at a single angle of incidence. In this paper, we will present results on applications of scalar models and vector diffraction theory to the analysis of both spectroscopic ellipsometry (SE), and spectral reflectometry (SR) data from patterned structures. Strong potential of specular measurements for topographic monitoring is indicated.

Experiments

We fabricated two types of experimental samples for tests of reflection models.

The first was a set of relief grating etched in (100) orientation single crystal Si wafers. Gratings with nominally equal lines and spaces were fabricated with periods of 2, 4, and 10 μm. The grating areas were 2.5 x 2.5 mm. They were etched by first patterning approximately 1.3 μm of Shipley 1813 photoresist using contact photolithography. The patterns were then etched using a Lam 9400 SE TCP high-density plasma etch tool. The etch conditions were: 10 mTorr pressure, an etch gas mixture of CL_2 (100 sccm) and HBr (100 sccm), a TCP power of 350 W, and a bias power of 160W. With this recipe, the etch rate is approximately 0.4 μm/min. Six wafers were etched to different depths (approximately100 to 600 nm in 100 nm increments) by changing the etching time. Due to time limitations, we concentrated our analysis efforts on the 500nm deep grating. We used the other wafers to simulate *in situ* data from the etching process. Post-etch cross-section scanning electron microscopy (SEM) was used to evaluate the line structure profile on the 500 nm sample (shown in Figure 1). There is no visible surface roughness and the lineshapes can be modeled as trapezoidal. There appears to be some concave-down rounding of the bottoms of the grating. This may have some influence on the results of our attempts to fit optical data from these structures.

Figure 1. Cross-sectional view of 4 μm period Si relief grating. We estimate the structure as: period=3.96 μm, top linewidth = 2.2 μm, depth = 0.52 μm, and wall angle = 73.9º.

The second set of samples was a set of aSi:H on Cr on glass samples from our flat panel display efforts. The samples contain no array structures within each die. The die are square and have a repeat distance of about 360 μm. Approximately 100 nm of Cr was deposited by magnetron sputtering on Corning 1737F glass substrates. The aSi:H was deposited using a PlasmaTherm Clusterlock 7000 PECVD chamber. The aSi:H patterns were etched using conventional photolithography and selective wet chemical etching.

All SE and SR measurements were performed on a Sopra GESP-5 spectroscopic ellipsometer/photometer system. The rotating polarizer ellipsometric measurements were performed in the tracking analyzer mode. For grating measurements at an angle of incidence of 75°, focusing optics were used to reduce the spot size so that only the grating was measured. For near-normal ellipsometry and reflectometry, an aperture was used to reduce the spot size. For measurements of the aSi:H samples, the full spot size of the instrument was used. Polarization-dependent reflectometry measurements were conducted in a double beam mode with a straight-through calibration of the instrument before each measurement.

Modeling and Simulation

For scalar analysis, we are using the modified Heimann approach (4) of the Lucent group (6). For diffraction analysis, we are using both commercial grating simulation software (12) which uses the rigorous coupled wave analysis (RCWA) method (13) and our own software which uses a surface integral equation (SIE) method (14).

The scalar model assumes that the profile of a patterned wafer is divided into separate uniform thin film regions. The total reflection coefficient of the structure is calculated as a complex combination of the individual reflection coefficients from the different regions, i.e.,

$$R_p = \sum_{i=1}^{2} af_i \exp\left(2j\frac{2\pi}{\lambda}\delta_i \cos(\phi_0)\right) R_{p_i} \qquad (1)$$

$$R_s = \sum_{i=1}^{2} af_i \exp\left(2j\frac{2\pi}{\lambda}\delta_i \cos(\phi_0)\right) R_{s_i}$$

where R_{p_i} and R_{s_i} are the reflectances in the p and s polarization corresponding to the i-th region. The nonnegative real number af_i is the area fraction of the i-th region. In Eq. (1), δ_i is the thickness of a layer of vacuum added on top of the i-th region to consider the phase lag due to the different heights of the stacks. Now, as usual, the ratio of R_p and R_s determines $\rho = \tan(\Psi)e^{j\Delta}$. The coefficients R_{p_i} and R_{s_i} are well-known nonlinear functions of the thickness of the layers in each stack (15). The computational load of this model is equivalent to the requirements of four different models for blanket wafers and is negligible compared with the vector diffraction models.

The RCWA algorithm finds a set of inhomogeneous plane waves which approximate the exact solution of the Maxwell's equation boundary value problem defined by the grating. The set of differential equations is solved with standard difference equation - eigenmatrix methods. Arbitrarily complex grating line profiles are approximated with discrete slices. The number of slices, s, and the number of plane waves (the order of algorithm, N) determines the computation time/wavelength point and simulation precision. A 2(N+1)s x 2(N+1)s matrix problem is created, but can be solved relatively efficiently due to the 4s x 2s block diagonal character of the matrix. For ellipsometry simulations, the complex *s*- and *p*-polarization fields were first computed and the tan(ψ) and cos(Δ) quantities were computed from these fields. In all our RCWA simulations, we used 10 slices to approximate the grating profiles. One limitation of the current software is that it will not use pointwise optical refraction indexes. To overcome this difficulty, we fitted silicon's *n* and *k* by a 10^{th} order polynomial (the maximum the software allowed). This introduced about 3% error in the worst region. The order, N, for our simulations was determined on the basis of energy conservation, and was typically in the range of 45-65. Our typical run times were on the order of 2.1-5.4 minutes/wavelength on a 300 MHz Pentium II™ system (so that a 100 wavelength SE simulation for a given structure could take up to 9 hours). Parallel computation can offer great time advantages but was not pursued in this initial effort.

The SIE algorithm uses a number of surface current filaments placed at the boundary between two media (air and Si in our case). By utilizing the equivalence theorem (a generalization of Huygen's Principle) and a two-dimensional periodic Green's function as a kernel, the diffracted field above and below the Si surface can be convoluted to form a single integral equation. By matching boundary conditions, the continuity of tangential components of both the E and H fields, the amplitude and phase of each surface current filament can be solved. The field of each diffraction mode can then be evaluated by the interference from these secondary filament sources. The typical execution times for this algorithm were 1.3 minutes/wavelength using 16 filament/(wavelength spacing on the grating) on a Sun Ultra Sparc 1 workstation.

In comparison with RCWA, the SIE approach uses fewer unknowns, and thus reduces the size of the variable matrix. Also, the most time-consuming part in the SIE algorithm, the evaluation of the periodic Green's function, must only be calculate once for both s and p polarization. Therefore, this method is much more computationally efficient than RCWA. To date, we have only been successful in applying the SIE model to the normal incidence case. A program including oblique incidence is under development and will be reported in a future publication.

Experimental Results

For the scalar analysis of the aSi:H/Cr/glass samples, the structure was divided into two thin film regions. We have included a native SiO_2 layer on top of the wafer. In addition, based on SE measurements of unpatterned aSi:H films on these substrates, we have inserted a thin surface roughness layer between the aSi:H and the Cr substrate. The refractive index of this layer was calculated with Bruggeman's effective media approximation using 50% of amorphous silicon and 50% of Cr.

We have measured $\tan(\Psi)$ and $\cos(\Delta)$ at an angle of incidence of $75°$. The cost function used to fit the model was as follows:

$$\sum_{\lambda}\left[\begin{array}{l}(\tan(\Psi)-\tan(\hat{\Psi}))^2+((\cos(\Delta)-\cos(\hat{\Delta}))^2+\\ (\frac{\partial(\tan(\Psi)-\tan(\hat{\Psi}))}{\partial\lambda})^2+(\frac{\partial(\cos(\Delta)-\cos(\hat{\Delta}))}{\partial\lambda})^2\end{array}\right] \quad (2)$$

where $\tan(\hat{\Psi})$ and $\cos(\hat{\Delta})$ are the estimates given by the model. The behavior of the patterned sample in the short wavelength range is very similar to bare Cr. Hence, we needed to include in Eq. (2) the error in the derivatives to force the model to fit the oscillations observed in the long wavelengths. These oscillations are not present in the bare Cr, and they are a distinctive characteristic of the patterned structure. Figure 2 shows the results of this procedure.

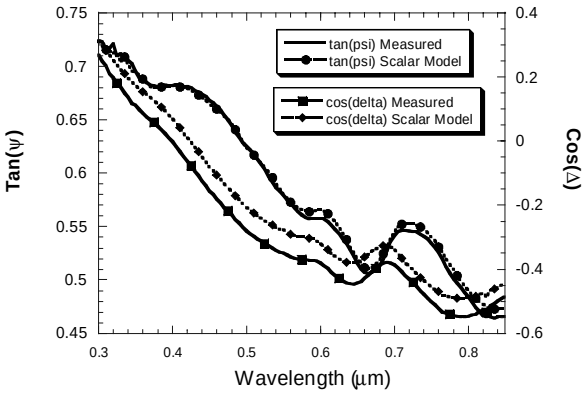

Figure 2. Measured SE data and fit of the scalar model for the aSi:H test structure. Model parameters: region 1- 10.96% (94.52Å SiO2 / 2888.42Å a-Si / 197.09Å roughness / Cr); region2- 89.04% (8.89Å roughness / Cr).

The model is in near-perfect agreement with the experimental data for $\tan(\Psi)$. Moreover, the area fraction of region 1 obtained by the model is very close to the nominal area fraction deduced from SEM measurements (about 9.3%). However, the scalar model shows an almost constant offset in $\cos(\Delta)$. This effect is evident in the data presented by the authors of (6) as well. This difference may be due to diffraction effects even though the pattern repeat distance is very long for these samples.

On the grating structures, SE data were collected from several die on the 500 nm depth sample at 75º. Typical data are illustrated in Figure 3. Data were collected both with the plane of incidence normal to the grating and parallel to the grating. As expected, we observed the strongest grating induced structure in the SE data for the case normal to the grating direction. We observed significant differences in the SE data curves between different die which we believe to due to small differences in the etch depth across the sample. As very long times are required for the RCWA simulation, we concentrated our data analysis efforts on an arbitrarily selected single 4 μm period grating the normal-to-the-grating geometry.

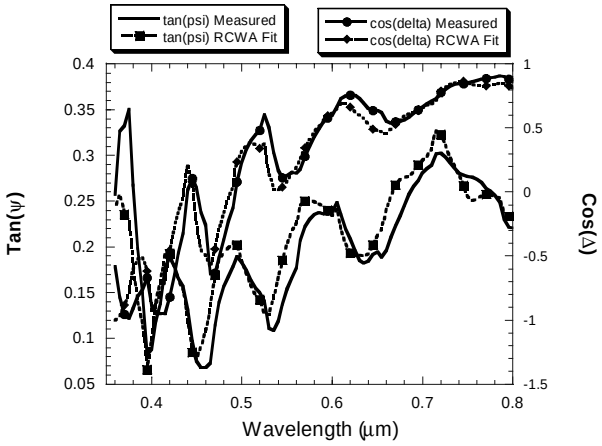

Figure 3. Measured SE data from the 500 nm depth, 4 μm period sample. The plane of incidence was normal to the grating. The RCWA simulation yielded a period of 4.0 μm, a top linewidth of 2.22 μm, a sidewall angle of 72.5º, and a depth of 480 nm.

Our RCWA simulations show several general trends. The positions of peaks and valleys in the oscillations in $\tan(\psi)$ and $\cos(\Delta)$ vs. λ are very sensitive to the period of the grating, while the magnitudes of both ellipsometric parameters were very sensitive to the structure depth. More subtle but still strong structures in the curves are related to the details of the lineshapes. However, these effects are not mutually orthogonal, so it is not a straight-forward exercise to extract the topography information from even these simple test structures. Samples with additional thin film structure would present even stronger challenges.

Therefore, we used a hybrid procedure for finding approximate fits to the grating topography. We measured both near-normal (6º) s- and p-polarized SR and SE data, and 75º SE data. Simple scale theory allow the thickness to be estimated from ¼ wave interference between waves reflected from the top and bottom of the grating:

$$\frac{1}{4d} = \left(\frac{1}{\lambda_{peak}} - \frac{1}{\lambda_{valley}} \right) \qquad (3)$$

We used this estimate on the p-polarized data as it is expected that these data will be less strongly influenced by coupled mode effects (16). We observed that the scalar-area fraction model could be applied to the p-polarized reflectance data to achieve very good fits, but that the s-polarized data showed stronger differences vs. the scalar model. Thus, for more complex samples, the scalar approach could be used on p-polarized normal-incidence reflectance data to establish initial guesses. These thickness estimates can then be refined, and linewidth and sidewall slope estimates can be added by iteratively fitting using the SIE approach. Finally, these estimates can be further refined using the RCWA algorithm.

The best fits we have achieved to the near-normal incidence data are shown in Figure 4 and Figure 5. The 75º SE data and RCWA simulation are illustrated in Figure 3. The agreement between the SEM-measured quantities and the ones from fits to optical data is good. The differences may be due to the differences between the two die, incomplete optimization of the RCWA analysis, magnification calibration errors in the SEM, or human error in measuring the SEM photo.

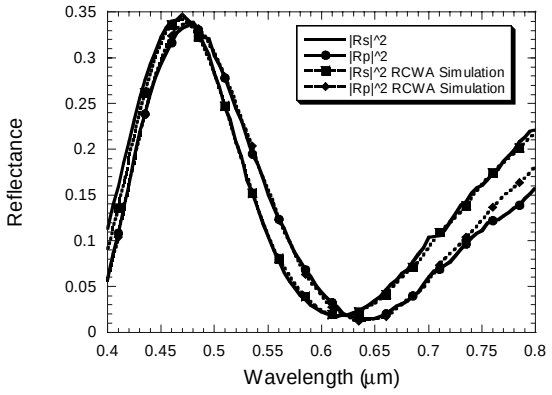

Figure 4. Measured and fitted s- and p-polarized reflectances at 6º for the nominal 500 nm deep, 4 μm period structure. The RCWA simulation yielded a period of 4.0 μm, a top linewidth of 2.22 μm, a sidewall angle of 72º, and a depth of 480 nm.

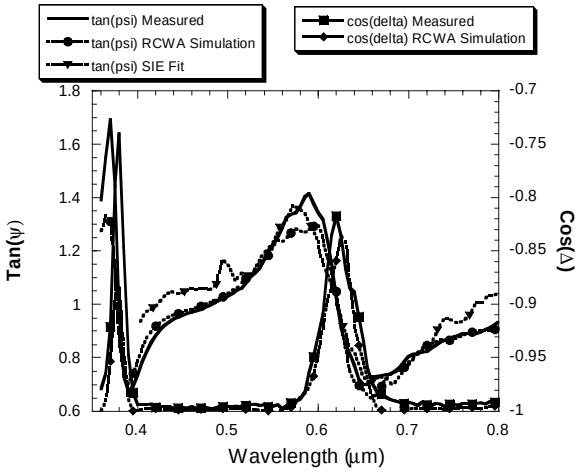

Figure 5. Near-normal (6º) SE data, SIE fit to tan(ψ) data, and RCWA simulation.

The potential of SE to measure evolving grating topographies during an etch was simulated by measuring the samples etched for varying times. We have not yet fully optimized the RCWA simulations for these experiments, but as can be seen in Figures 6 and 7, the basic trends in the experimental data are reflected in the modeled results. Careful examination of the side-by-side simulations and experiments reveals similar non-monotonic behavior in both tan(ψ) and cos(Δ) as the etch depth increases. In this simulation the top and bottom linewidths were held constant at 2.2 and 2.5 μm, respectively, and the period was held constant at 3.96 μm. This leads to a varying wall angle. A constant wall angle simulation may lead to more comparable results to the experimental data. By more accurately fitting theory to experimental data, it should be possible to accurate extract etch depth and wall vs. etch time from in situ data. Other RCWA simulations which we have made for 0.1 μm line/space gratings indicate that this technique will be applicable for monitoring the etching of deep submicron structures.

Conclusions

Use of SE and/or SR yields quantitatively accurate critical dimension and wall angle data on patterned semiconductor structures. These methods can be employed for *in situ* monitoring and process control. However, accurate analysis requires both good prior knowledge of the approximate structure and computationally-intensive vector diffraction calculations. Use of successively more complex but accurate approximation techniques can reduce the need for prior knowledge. Scalar simulation techniques show promise for locally irregular structures, but some method to account for polarization-dependent scattering appears to be necessary even in these cases.

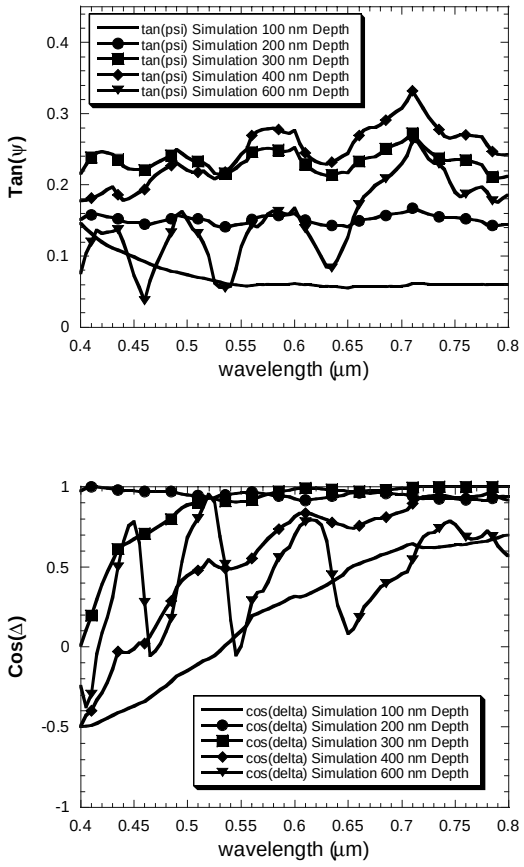

Figure 6. Simulated tan(ψ) (top) and cos(Δ) (bottom) curves at 75º angle of incidence for a series of etched 4 μm period Si gratings.

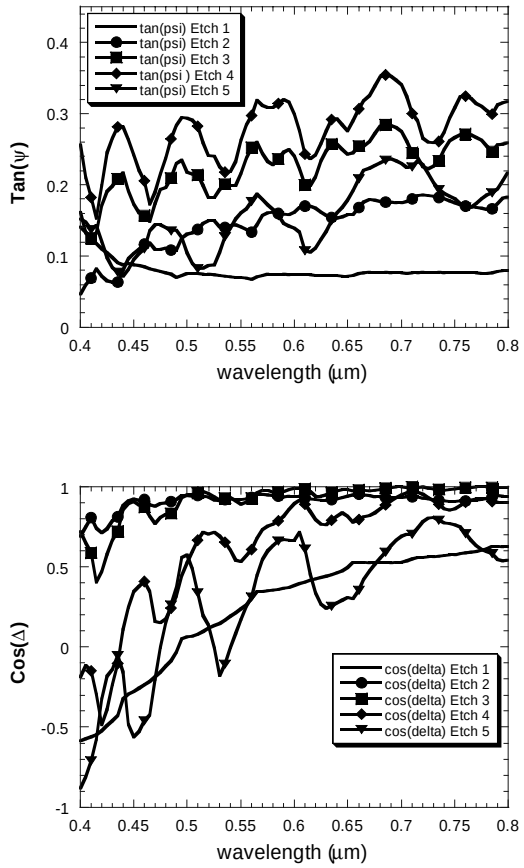

Figure 7. Experimental tan(ψ) (top) and cos(Δ) (bottom) curves at 75º angle of incidence for a series of etched 4 μm period Si gratings.

Acknowledgements

This work was supported in part by the Semiconductor Research Corporation (contract 97-FC085), AFOSR/DARPA MURI Center for Intelligent Electronics Manufacturing (AFOSR F49620-95-1-0524), and the State of Michigan Center for Display Technology and Manufacturing. The authors would also like to thank Dr. D. S. Grimard and Ms. M. Gulari for assistance with sample fabrication.

References

1. D.E. Aspnes, Solid State Communications, 101, pp.85-9 (1997)
2. T. L. Vincent, P.P. Khargonekar, and F.L. Terry, Jr., J. Electrochem. Soc., 144, pp.2467-72 (1997)
3. T. B. Benson, L.I. Kamlet, P. Klimecky, and F.L. Terry, Jr., J. Elec. Mat., 25, pp955-64 (1996)
4. P. A. Heimann and R. J. Schutz, J. Electrochem. Soc., 131, pp. 881-5 1984).
5. M. Haverlag and G. S. Oehrlein, J. Vac. Sci. Techn., B10, pp. 2412-8 (1992).
6. H. L. Maynard, A. N. Laydi, J. T. C. Lee, J. Vac. Sci. Tech., B15, pp109-15 (1997)
7. N. Blayo, R. A. Cirelli, F. P. Klemens, and J. T. C. Lee, J. Opt. Soc. Am., A 12, pp. 591-9 (1995).
8. D. W. Mills, R. L. Allen, and W. M. Duncan, Proc. SPIE, 2637, pp. 194-203 (1995).
9. H. Arimoto, Jpn. J. Appl. Phys., 36,pp. L173-5 (1997).
10. C.J. Raymond, M.R. Murnane, S.L. Prins, S.S.H. Naqvi, J.R. McNeil, J.W. Hosch, Proc. SPIE, 2725, pp.698-709 (1996)
11. T.M. Morris, D.S. Grimard, C.F. Shu, F. L. Terry, M.E. Elta, R.C. Jain, Proc.SPIE, 1926,pp.27-32 (1993)
12. Grating Solver Development Co., Allen, TX..
13. M. G. Moharam and T. K. Gaylord, J. Opt. Soc. Am., pp. 1385-1392 (1982).
14. R. Petit, ed., *Electromagnetic Theory of Gratings*, Springer-Verlag (Berlin, 1980).
15. Azzam, R.M.A. and Bashara , N.M., *Ellipsometry and Polarized Light*, Elsevier (Amsterdam, 1986).
16. D.A.Gremaux and N.C.Gallagher, Appl. Opt., 32, pp.1948-1953 (1993).